RSC Advances

PAPER

View Article Online
View Journal | View Issue

Cite this: *RSC Adv.*, 2022, **12**, 32708

Citrus limetta fruit waste management by liquefaction using hydrogen-donor solvent

Sneha Acharya and Nanda Kishore *

The liquefaction of *Citrus limetta* fruit waste (both pulp and peel) in a hydrogen-donor solvent has not been reported in the literature and authors considered the same as the objective of this work. Thus, results on waste management of this potential fruit wastes by liquefaction in hydrogen-donor methanol solvent at 260 °C temperature, residence time of 30 min, and 1 : 2, 1 : 3 and 1 : 4 biomass-to-solvent ratios were reported in this work. The aim was to achieve biofuels of high quantity and quality from this waste, which would otherwise be disposed of without any value addition. A maximum of 12.5 wt% of biocrude yield was found from *Citrus limetta* peel biomass, which was higher than that from the thermochemical conversion of other citrus fruit waste biomasses. Biocrude having higher heating value (HHV) of 26.76 MJ kg^{-1} from *Citrus limetta* pulp, when the feed biomass pulp-to-solvent ratio was 1 : 4, found to be the best outcome of this study. Biocrude and biochar have also been extremely characterized using several advanced techniques such as Gas Chromatography Mass Spectrometry (GC-MS), Fourier Transform Infrared Spectroscopy (FTIR), and Field Emission Scanning Electron Microscopy (FESEM), etc. Finally, the novelty of this work is not only obtaining higher yield of biocrude but also better HHV compared to other similar studies in the literature.

Received 27th September 2022
Accepted 1st November 2022

DOI: 10.1039/d2ra06085j

rsc.li/rsc-advances

1. Introduction

The last century has witnessed unprecedented industrial and urban developments, which continue till date. This is evident from the wide acceptance and utilization of new generation technologies, thereby increasing the demands of the ever rising urban population. The sole dependence on existing conventional energy resources is facing serious threat; thus, shifting towards new and renewable alternatives is the need of the hour. Biomass, which is a term used for organic matter of both animal and plant origin, is being widely studied for its applications as a renewable energy resource in recent times.[1] This has occurred due to its wide availability and carbon-neutral nature. Materials such as agriculture and forestry wastes, animal residues, residues from food processing industries, and municipal solid wastes can be considered as potential biomass resources.[2] Apart from having almost zero cost of procurement, their use ensures the implementation of proper waste management disposal strategies, which is the greatest issue of urban dwellings in recent times. Both biochemical and thermochemical conversion technologies[3,4] are being extensively researched for biofuel production from biomass.[5,6] Thermochemical conversion comprises of gasification, pyrolysis, and hydrothermal processing. Hydrothermal processing is further divided into hydrothermal liquefaction, hydrothermal carbonization, and hydrothermal gasification. These processes are promising as wet biomass feedstock can be directly converted to biofuels without the involvement of any energy consuming drying or pretreatment.[7] Thus, the reason for undertaking liquefaction studies of biomass by the authors is because they provide an edge over other thermochemical conversion technologies.

The conversion of wet biomass at moderate temperature range (280–375 °C) in water and high pressure range (5–25 MPa) to obtain desirable liquid (biocrude) having a high energy content, solid (biochar), and gaseous products is called hydrothermal liquefaction (HTL).[8–10] The biocrude is a composite blend of compounds, while biochar represents the char that is insoluble in organic solvents. The separation of the biocrude and char is conducted using an organic solvent in laboratory-scale operations. This solvent ideally possesses similar polarity to that of the compounds proposed to be found in raw biocrude.[2] Liquefaction with water as well as organic solvents has been reported in the literature[11–18] to boost the yield of liquid products. Nonetheless, further investigation is required on the use of solvents with high polarity due to their advantages from the perspective of product yield. These solvents also aid in the fruitful utilization of hydrogen and carbon compounds in it, thus leading to value-added hydrocarbon formation along with the upsurge in the percentage of aliphatic esters in the biocrude.[19] Therefore, to simplify the adversity of the conditions in which HTL is carried out, researchers have tried to utilize a hydrogen-donor solvent such as organic acids to enhance the

Department of Chemical Engineering, Indian Institute of Technology Guwahati, Guwahati-781039, Assam, India. E-mail: nkishore@iitg.ac.in; mail2nkishore@gmail.com

liquid product yield.[11–13,15–17,20–23] Among the various solvents, the high polarity solvent acetone was inefficient in the proper conversion of cellulose as it failed in the donation of active radicals that are responsible for stabilizing undesirable reaction intermediates formed during the liquefaction reaction. Similarly, non-polar solvents have also showed their incapability as a hydrogen-donor, portraying a poor ability for solvolysis on cellulose conversion. They have also proved to be unsuccessful in the breakage of the intermolecular and intramolecular hydrogen bonds.[15] However, one such hydrogen-donor solvent having the ability to stimulate better raw material conversion is methanol (polarity = 0.762), which has the potential to promote solvolysis along with the breakage of the polymer chain of the cellulose components to enhance the destruction of their crystalline regions.[24] The intermediates formed during cellulose conversion were stabilized by hydrogen radicals from methanol to enhance the yield of biocrude.[25] Thus, methanol solvent was chosen as a hydrogen donor for biomass liquefaction by the authors.

Waste generation from food processing industries has been a matter of concern from the environmental, economic, and social point of view. Understanding the food supply chain network, it can be realized that this type of wastage is more prevalent during the consumption and manufacturing stages. This makes their effective disposal an important issue to be looked upon by emerging waste management technology developers.[26,27] Citrus fruits are widely consumed and very popular during the summer season in the Indian subcontinent due to the nutrition as well as the refreshment they provide. Sweet lime, commonly known as Mosambi and scientifically as *Citrus limetta*[28,29] (CL), is consumed for its juice, thereby generating lots of waste in the form of peel and pulp (after juice extraction). This fruit waste is extensively available after juice extraction and is disposed of as a waste without any value addition to it. Recently, several waste management strategies have been implemented to look into this matter. The hydrothermal liquefaction of food wastes,[30,31] more particularly fruit wastes,[2,32–36] is currently being developed, but its pace is quite slow. The state of the art establishes that researchers have been using CL peel as an adsorbent for heavy metal[37] and methylene blue dye[38] removal from water. Besides, the biochar obtained from these peels has also been used as an adsorbent for the removal of lead from battery manufacturing industrial effluent.[39] Biodiesel production from CL seed oil by simple transesterification process[40] and pyrolysis of such citrus fruits[41,42] has paved the path for their utilization in other thermochemical conversion processes. Moreover, none of these studies deal with the liquefaction and extensive product analysis of CL fruit waste. This motivated the authors to decide upon the novelty of this work to investigate the liquefaction of CL fruit waste (both pulp and peel) in a hydrogen-donor solvent and the thorough characterization of the products obtained. The products were analyzed for their yield along with the investigation of their physicochemical properties and energy content. In addition, other characterization techniques such as Nuclear Magnetic Resonance Spectroscopy (NMR), Gas Chromatography Mass Spectrometry (GC-MS), and Fourier Transform Infrared Spectroscopy (FTIR) of the biocrude have been used for the determination of the functional groups, molecular identity, and structure of molecules. Further, for the solid product, Field Emission Scanning Electron Microscopy (FESEM), X-ray Diffraction (XRD), and thermogravimetric analysis (TGA) studies along with energy content determination were done to investigate their applications as a fuel source.

2. Materials and methods

2.1 Materials

Sweet lime or *Citrus limetta* wastes (juice extracted pulp and peel) were collected from a juice shop within the academic complex of IIT Guwahati, Assam, India campus. The collected pulp sample was further vacuum filtered to remove any remaining juice from it, while the peel was used as it was. The seeds from the pulp sample were removed to maintain the homogeneity of the feedstock being used. Methanol (CH_3OH) solvent that was used was reagent grade chemical (Make: Merck).

2.2 Experimental procedure

Liquefaction of *Citrus limetta* pulp and peel waste biomass was done in a batch stirred autoclave reactor (Make: Lelesil, India) of 500 mL volume, whose schematic diagram has been shown in Fig. 1. CL pulp (CLPU) biomass along with the solvent, *i.e.*, CH_3OH, was fed to the reactor at 1 : 2, 1 : 3, and 1 : 4 biomass-to-solvent ratios. These biomass-to-solvent ratios were selected on the basis of changing biomass weight method where the amount of biomass was changed in each case while fixing the amount of the solvent. Thereafter, the reactor was positioned within the furnace possessing 15–20 °C min^{-1} heating rate. Then, the reactor was closed properly and the fittings were checked and tightened to ensure that no leakage occurred during the reaction. At first, 20 bar of N_2 was purged through the reactor and leak tests were performed to identify any leakage that might exist in the reactor fittings and hamper the results obtained. Thereafter, N_2 gas was completely released from the reactor prior to furnace heating. The desirable reactor temperature was set to 260 °C and stirring speed of the rotor was set to 200 rpm to begin the reaction. The system pressure was allowed to escalate freely until the temperature of the reaction was achieved. The reactor was held for 30 min residence time at the same reaction temperature. It was observed that the pressure within the reactor during the reaction time remained within 90–100 bar.

The selected reaction conditions were specific to the equipment specifications and literature review[30,32,43,44] and were finalized on the basis of the test runs in the lab-scale setup. However, it should be noted that it was not possible to conduct the experiments at a biomass-to-solvent ratio below 1 : 2 (by increasing the amount of methanol beyond 100 mL) because then the pressure of the liquefaction reaction would have exceeded the limit of the reactor specifications. The furnace was switched off at the end of the residence time and then the reactor was quenched immediately by an ice water circulating pump to reduce the reactor temperature by 80–100 °C in 5 min.

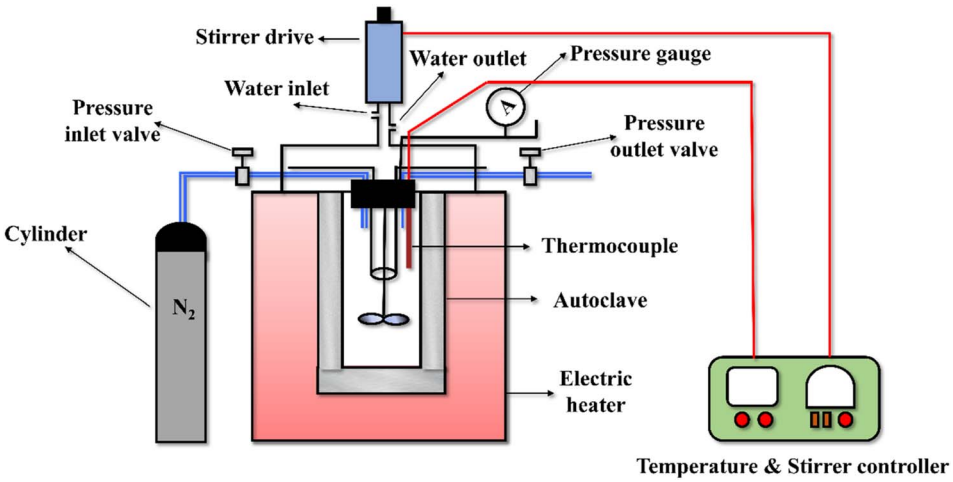

Fig. 1 Schematic diagram of the stirred autoclave reactor setup.

The products inside the reactor were a mixture of semi-viscous liquid and solid char that were extracted as per the procedure adapted from the literature.[22,45,46] They were subjected to filtration with a Whatman 40 filter paper using a vacuum pump until all the liquid was separated from the solid residue. This filtrate was analyzed for its physical properties and HHV, and then stored separately for solvent extraction. Meanwhile, the reactor interior and the stirrer were washed with 40 mL acetone to remove any sticky or greasy product adhered to them. This was collected and stored in a separate sample bottle. The filter paper having the solid residue was further subjected to Soxhlet extraction using acetone to remove any greasy viscous substance stuck to them. The remaining acetone after extraction was also stored along with the acetone that had been used for washing for further processing. The solid residue termed as biochar was dried at 103 °C in a hot air oven for 3 h and stored properly for further characterization. Thereafter, the filtrate was taken in a pear-shaped round bottom flask and evaporated at 60 °C in a vacuum rotary evaporator under reduced pressure to remove the unreacted methanol solvent from it in a separate collection flask. This was termed as remaining methanol solvent (MSR). The volume of the MSR was recorded and it was stored for further analysis. After methanol solvent removal, some dark and viscous liquid could be seen to be remaining in the round bottom flask. Then, the acetone that was used for reactor washing as well as that obtained from Soxhlet extraction was further added to this flask, and the evaporation of the solution was done to remove the acetone and aqueous part of the product liquid to get a highly viscous and sticky bitumen-like product that was termed as "biocrude" and was stored for characterization.[47–50] However, it was possible that some light hydrocarbons might have evaporated during solvent and water removal from the biocrude. The same reaction procedure was repeated using CL peel (CLPE) biomass at 1 : 2, 1 : 3, and 1 : 4 biomass-to-solvent ratios and 260 °C temperature. The yield of the filtrate and biochar obtained in wt% was the ratio of the product found to that of the raw feed material as well as the solvent. The total yield of the gaseous products, aqueous phase products, and losses incurred through solvent retrieval were termed collectively as the "yield of others", which was found by difference of 100% from the percentage yield of filtrate and biochar.[18] However, the yield of the biocrude obtained in wt% is the ratio of biocrude obtained after solvent separation to that of the raw feedstock used. The experiments were done in triplicates for each of the biomass-to-solvent ratios and the average values of the product yield was reported.

2.3 Feedstock and product characterization

The proximate analysis of CLPU and CLPE biomass to investigate its moisture content (MC), volatile matter (VM), ash content, and fixed carbon (FC) content was carried out. The ultimate analysis of the biomass in CHNS elemental analyzer (EuroEA3000, Euro Vector, Italy) provided its mass% of elemental composition. The oxygen percentage in the biomass was found by deducting the C, H, N, and S content in mass% from 100, *i.e.*, O (mass%) = 100 − (C mass% + H mass% + N mass% + S mass%). A bomb calorimeter setup (Make: HAMCO instruments Pvt. Ltd., India) was utilized to calculate the higher heating value (HHV) of biomass, biocrude, and biochar. The physicochemical and fuel characteristics analysis of the liquid (filtrate) obtained after liquefaction and MSR was done to determine their pH, viscosity, density, and higher heating value (HHV). Solvent removal using a rotary evaporator (Rotavapor, R 300, Make: Buchi, Switzerland) was done to obtain MSR and biocrude. The degradation pattern of biomass as well as biochar was found by thermogravimetric analysis (TGA), followed by differential thermogravimetry (DTG). The TGA equipment (TG 209 F1 Libra, Netzsch, Germany) was used within 25 °C to 900 °C range of temperature with 10 °C min^{-1} heating rate with N_2 gas purging to obtain volatility and thermal stability of the biomass sample. The biocrude was subjected to FTIR spectroscopy to examine the existing functional groups in them. The instrument used Shimadzu IR solutions software 1.5 and was set in the 400–4000 cm^{-1} wavenumber range for 30 scans with 4 cm^{-1} spectral resolution. FTIR analysis was established by

investigating the probable structure of the chemical compounds in biocrude by proton Nuclear Magnetic Resonance Spectroscopy (^{1}H NMR, 600 MHz, Bruker, USA) using chloroform-D solvent and 16 scans for proton. Gas Chromatography Mass Spectrometry (GC-MS, PerkinElmer Clarus 680 GC/600C MS) was used to study the possible chemical compounds in the biocrude from the liquefaction of CLPU and CLPE biomass. A capillary column that was layered with a film of 250 μm and length of 60 m was used. It had a split injector with a split ratio of 10 : 1 at 280 °C. Carrier gas He of 99.95% purity at 1 mL min^{-1} flow rate was employed. The GC oven was set to 40 °C temperature for 2 min initially and then ramped at 10 °C min^{-1} to 140 °C, where it was held for 2 min. Finally, the ramp was reduced to 7 °C min^{-1} to reach 300 °C and held for 5 min. The National Institute of Standards and Technology (NIST) 2014 MS library was referred to detect the compounds present in the biocrude. X-ray diffraction (XRD) for the biomass and biochar samples was carried out to determine their crystalline and amorphous nature with the 2θ values ranging from 10° to 90° in XRD equipment (Rigaku, Japan) using X-ray radiation of Cu-Kα. The surface morphology of the biomass and biochar was studied by high-resolution imaging in a Field Emission Scanning Electron Microscope (FESEM), Gemini model (Make: Zeiss, Germany), where the images were taken at 2k×, 5k×, and 10k× magnification.

3. Results and discussion

3.1 Analysis of biomass

The proximate analysis of CLPU and CLPE (as received basis) along with its HHV has been depicted in Table 1. Both biomasses had a high MC of >20 wt% as they were directly used for liquefaction without any prior drying or heat treatment. Both CLPU and CLPE had high VM content of 61.33 wt% and 66.35 wt%, respectively, which was actually an affirmative indication from the biocrude yield point of view as biomasses with high VM get devolatilized easily along with the production of less amount of char.[42] The amount of inorganic compounds present in the biomass was detected by its ash content. In both the biomasses, the ash content was almost similar to other fruit wastes (pomace and peels).[42,51,52] The FC content of CLPU was less than 10.5 wt%, indicating that the biochar yield was less than that of biocrude. Both the biomasses had HHV values that were in close conformity with other lignocellulosic biomasses[5,53] and fruit wastes.[2,42,51] The ultimate analysis of CLPU showed 43.16 wt% of elemental carbon composition, which was comparable to 38.51 wt% of similar citrus biomass waste.[51] The hydrogen content was also in range with other lignocellulosic biomasses. The H/C ratio of CLPU and CLPE was 1.568 and 1.772, respectively, and was consistent with similar fruit waste biomasses.[2,42,51] However, the O/C ratio of 0.855 and 0.873 for CLPU and CLPE, respectively, was slightly lower compared to other similar biomass,[42,51] which added value to CLPU and CLPE for utilizing them as a source for the production of biocrude.

Thermogravimetric analysis (TGA) and differential thermogravimetry (DTG) curves of CLPU and CLPE biomass was shown in Fig. 2. Within temperature range of 30 to 100 °C, water molecules adsorbed on the surface of both the biomass samples as well as those bound within the inner cells underwent

Table 1 Proximate and ultimate analysis of biomass samples and their HHV

	Proximate analysis, wt%				
Biomass feedstock	MC	Ash	VM	FC[a]	HHV, MJ kg^{-1}
CLPU	23.20	5.26	61.33	10.22	15.88
CLPE	24.57	6.18	66.35	2.89	13.81

	Ultimate analysis, wt%						
Biomass feedstock	C	H	N	S	O[a]	H/C	O/C
CLPU	43.16	5.64	2.02	—	49.19	1.568	0.855
CLPE	42.60	6.29	1.56	—	49.56	1.772	0.873

[a] Calculated by difference.

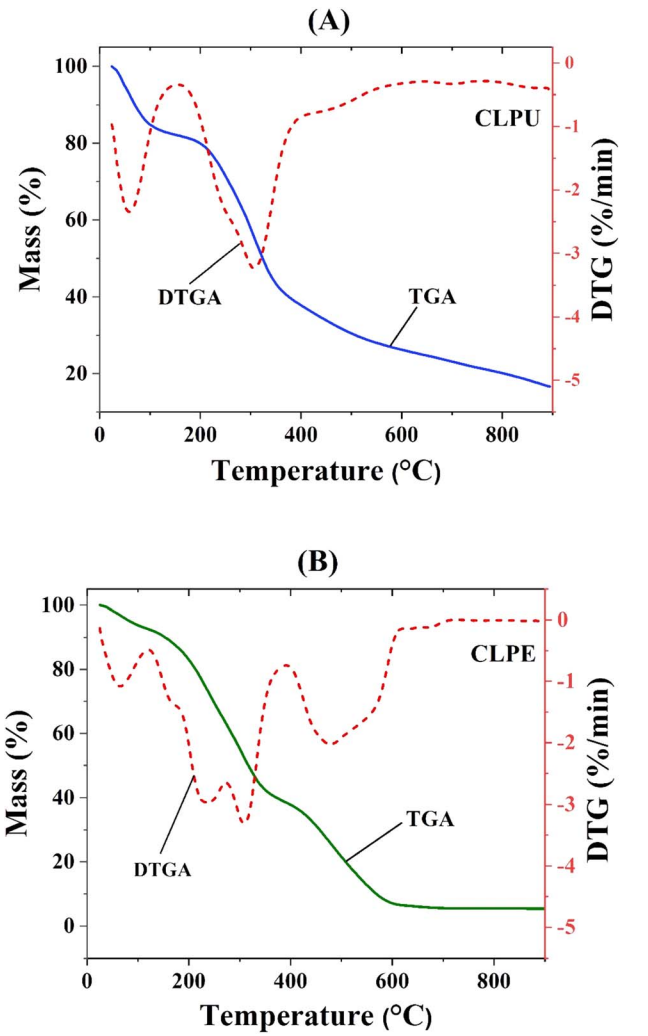

Fig. 2 Thermogravimetric analysis and differential thermogravimetry plot of (A) CLPU and (B) CLPE biomass.

dehydration to cause weight loss from 10–20 wt% that was common to other lignocellulosic biomass samples. Hemicellulose volatilization was observed between 200 and 400 °C with maximum weight loss at approximately 300–350 °C.[5] Firstly, the decomposition of less thermally stable volatile compounds occurred, leading to the breakage of their chemical bonds. Between 350 and 400 °C, overlap between cellulose and hemicellulose decomposition took place.[6] The loss of lignin content in CLPE was apparent from a long devolatilization tail at 440 °C temperature. A groove between 220 and 330 °C in the DTG profile indicated the degradation of hemicellulose and cellulose. A small groove at about 500 °C was proof of lignin degradation.[54] These plots were in agreement with the studies conducted on similar citrus fruit wastes.[42]

3.2 Product yield

Fig. 3 illustrated the yield of filtrate (wt%), biochar (wt%), and yield of others found from the liquefaction of both CLPU and CLPE biomasses in hydrogen-donor methanol solvent at 260 °C temperature and 1 : 2, 1 : 3, and 1 : 4 biomass-to-solvent ratios, respectively. It was observed that the variations in the biomass-to-solvent ratios led to the variation in the product yield from liquefaction. For CLPU biomass, the highest yield of the filtrate was obtained at 1 : 4 ratio. Similar trends were observed with CLPE biomass as well. However, the biochar yield was found to decrease for both biomasses with decreasing biomass-to-solvent ratios. This was an indication of the better conversion of organics in the biomass to liquid products under a solvent-rich environment. This low biochar yield might also be considered to be a characteristic of the fruit waste biomass being used. It is worth mentioning here that it becomes difficult for the comparison of the yield with literature due to the novelty of the feedstock being used in this research, in addition to the limited studies and documentation on liquefaction product yield with citrus fruit wastes. The yield of dark and highly viscous biocrude obtained from the vacuum evaporation of the

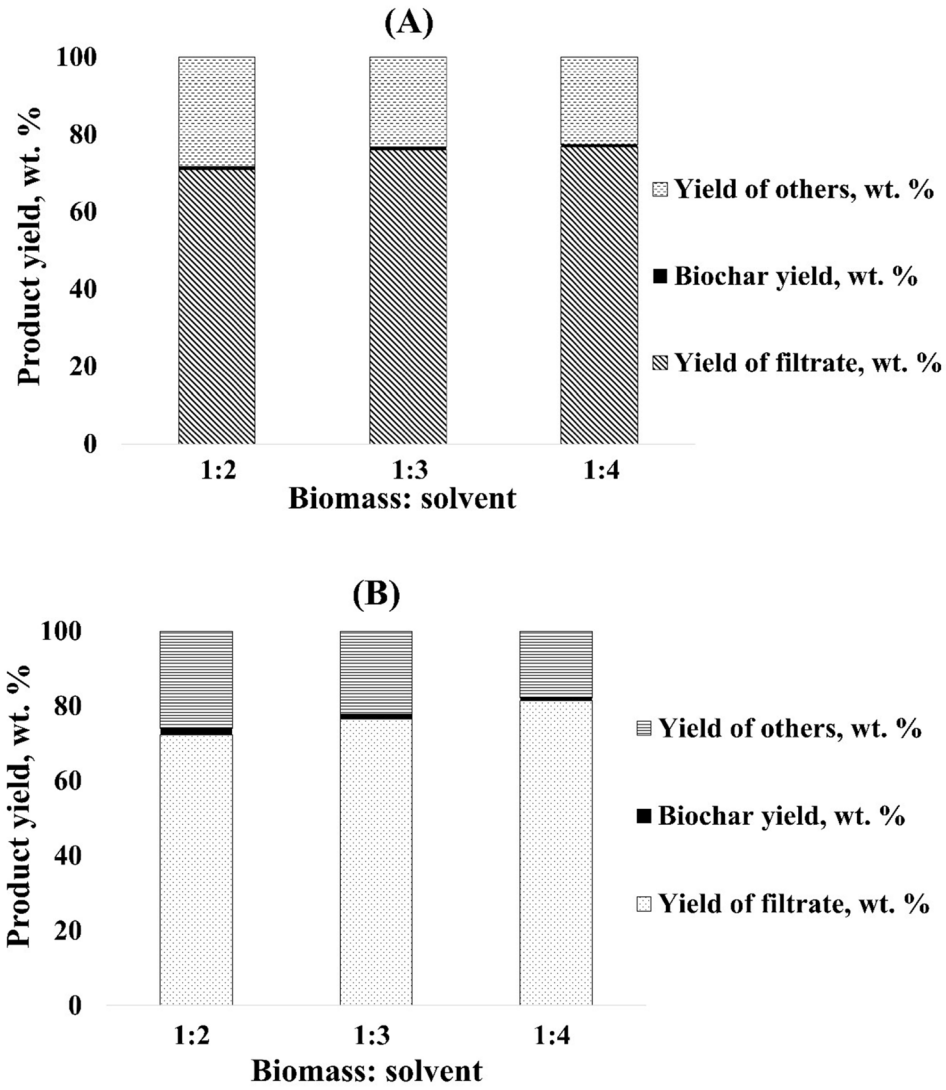

Fig. 3 Product yield from the liquefaction of (A) CLPU and (B) CLPE biomass with hydrogen-donor solvent methanol at 260 °C and 1 : 2, 1 : 3, and 1 : 4 biomass-to-solvent ratios.

solvent from the filtrate, the procedure of which has been discussed above (Subsection 2.2), was also calculated on wt% basis with respect to the feed being used for the reaction. However, this yield was found to increase with a decrease in the biomass-to-solvent ratio for both biomasses. A maximum biocrude yield of 7.88 wt% and 12.5 wt% was obtained with CLPU and CLPE biomasses, respectively. The reason behind this could be the reaction of the hydrogen-donor methanol solvent with the reaction intermediates produced from the liquefaction of CLPE biomass, thereby enhancing the biocrude yield from it. It may be noted that the biocrude yield obtained in this work was higher than that reported in the literature on the liquefaction of other citrus fruit wastes, wherein the yield was reported as 7.53 wt%.[32] Nonetheless, it becomes difficult to draw a general conclusion regarding the optimum biomass-to-solvent ratio to generate maximum biocrude yield because several other important reaction parameters such as operating temperature, reactor volume, residence time, pressure, feedstock type, cooling and heating rates, and particle size influence the biocrude yield to a large extent.[9,43] The pressure of the system that reached about 100 bar conducted a significant part in the product yield from liquefaction. The increase in the pressure led to the increase in the solvent density in the supercritical state, allowing better penetration of the solvent into the biomass, thus aiding its decomposition to extract the disintegrated products into the liquid phase.[55] The high pressure system also inhibited vaporization to allow the compounds to be in the liquid state.[43]

Table 2 Physical characteristics of the filtrate and MSR after the liquefaction of CLPU and CLPE at 260 °C and different biomass-to-solvent ratios

Product	1 : 2	1 : 3	1 : 4
Density, g mL^{-1}			
CLPU (Filtrate)	0.872	0.861	0.844
CLPU (MSR)	0.824	0.847	0.822
CLPE (Filtrate)	0.860	0.851	0.841
CLPE (MSR)	0.819	0.826	0.816
Density of pure reagent grade methanol, g mL^{-1} = 0.782			
Viscosity, mPa s			
CLPU (Filtrate)	1.182	1.178	1.038
CLPU (MSR)	0.899	1.074	0.913
CLPE (Filtrate)	1.155	1.142	1.040
CLPE (MSR)	0.938	0.918	0.883
Viscosity of pure reagent grade methanol, mPa s = 0.677			
pH			
CLPU (Filtrate)	6.98	7.15	7.12
CLPU (MSR)	7.45	7.60	8.19
CLPE (Filtrate)	6.22	6.38	6.72
CLPE (MSR)	6.6	6.82	7.15
pH of pure reagent grade methanol = 7.75			
HHV, MJ kg^{-1}			
CLPU (Filtrate)	18.40	14.89	16.09
CLPU (MSR)	16	15.89	17.69
CLPE (Filtrate)	15.16	16.23	17.19
CLPE (MSR)	17.58	17.36	17.41
HHV of pure reagent grade methanol, MJ kg^{-1} = 19.62			

3.3 Analysis of liquid products

3.3.1 Physical and fuel analysis. The physical characteristics and HHV of the filtrate and remaining methanol solvent (MSR) after the evaporation of this filtrate obtained from the liquefaction of CLPU and CLPE at 260 °C with hydrogen-donor methanol solvent at 1 : 2, 1 : 3, and 1 : 4 biomass-to-solvent ratios were investigated and have been listed in Table 2. The density of the CLPU filtrate decreased with increasing biomass-to-solvent ratio, and a comparable trend was detected in the situation of the CLPE filtrate. The density values of the filtrates obtained by the liquefaction of CLPU were slightly higher than those obtained by CLPE liquefaction regardless of the biomass-to-solvent ratio values. Similarly, the density values of the recovered methanol by evaporation of crude, *i.e.*, MSR of CLPU were slightly higher than those of CLPE irrespective of the solvent ratios. On the other hand, the density values of MSRs (both from filtrates of CLPU and CLPE liquefaction) were substantially higher than that of the pure solvent. This indicated that some of the lighter hydrocarbons of filtrates and/or methanol soluble components of filtrates obtained by the liquefaction of CLPU and CLPE were transferred to the MSR during evaporation process; thus, it cannot be reused as a solvent but may be used as a lighter fuel fraction.

The viscosity of the CLPU filtrate was found to decrease with increasing biomass-to-solvent ratio; the same was the case for the CLPE filtrate with each biomass-to-solvent ratio. The viscosity of MSRs were substantially lower than the filtrates of both CLPU and CLPE liquefaction, whereas the viscosity of MSRs of both CLPU and CLPE liquefaction were much higher compared to that of pure methanol solvent. Thus, it was again clear that MSR possessed same lighter fuel fractions and/or methanol soluble components of filtrate and cannot be reused as the solvent. In other words, the filtrate contains some lighter hydrocarbons whose vapor pressures are close to that of pure methanol solvent.

The CLPU and CLPE filtrates were found to be almost neutral, varying in the range from 6.2 to 7.2 approximately, which was a very positive outcome from the fuel potential viewpoint. The pH of the CLPE filtrate was found to increase from 6.2 to 6.7 as the biomass-to-solvent ratio increased, whereas mixed trends were obtained in the case of the CLPU filtrate. On the other hand, the pH values of MSRs of CLPU and

Table 3 Fuel potential of biocrude and biochar obtained by liquefaction at 260 °C and different biomass-to-solvent ratios

	HHV of biocrude, MJ kg^{-1}			HHV of biochar, MJ kg^{-1}		
Biomass feedstock	1 : 2	1 : 3	1 : 4	1 : 2	1 : 3	1 : 4
CLPU	26.36	26.7	26.76	16.98	16.46	16
CLPE	24.91	24.2	23.7	14.94	15.55	16.5

CLPE liquefaction were found to increase with increasing biomass-to-solvent ratio.

The HHV of the filtrate of CLPE liquefaction was found to increase with the biomass-to-solvent ratio, whereas mixed trends were found in the case of the CLPU filtrate. The HHV of MSR of both CLPU and CLPE liquefaction was found to be higher than either filtrate except in the case of CLPU with 1 : 2 ratio. This may be attributed to the increased penetration of the solvent into the biomass during the initial period of liquefaction with increasing biomass-to-solvent ratio.[43] On the other hand, the HHV of biocrude (final product after recovering MSR from filtrate) was found to be almost constant (or only marginally increasing) in the case of CLPU, whereas the opposite was true for CLPE with respect to the increasing biomass-to-solvent ratio. However, for a fixed value of biomass-to-solvent ratio, the HHV of CLPU biocrude was higher than that of CLPE (Table 3 and Fig. 4).

Finally, to summarize, the HHV of the biocrude obtained after solvent removal was comparable to those obtained from other lignocellulosic biomasses.[9] The probable reasons for HHV trends might be that in comparison to biomass, the biocrude had a higher content of carbon and a lower content of oxygen, resulting in HHV rise.[9] The dehydration, decarboxylation, and decarbonylation reactions occurring during liquefaction was the key factor behind the decline in the oxygen content in biocrude. Moreover, an increase in the hydrogen content occurred due to the generation of active hydrogen by supercritical methanol and its integration in the biocrude.[7] Nonetheless, the biomass-to-solvent ratio should be adjusted with utmost care to get an optimum yield of biocrude with optimum heating

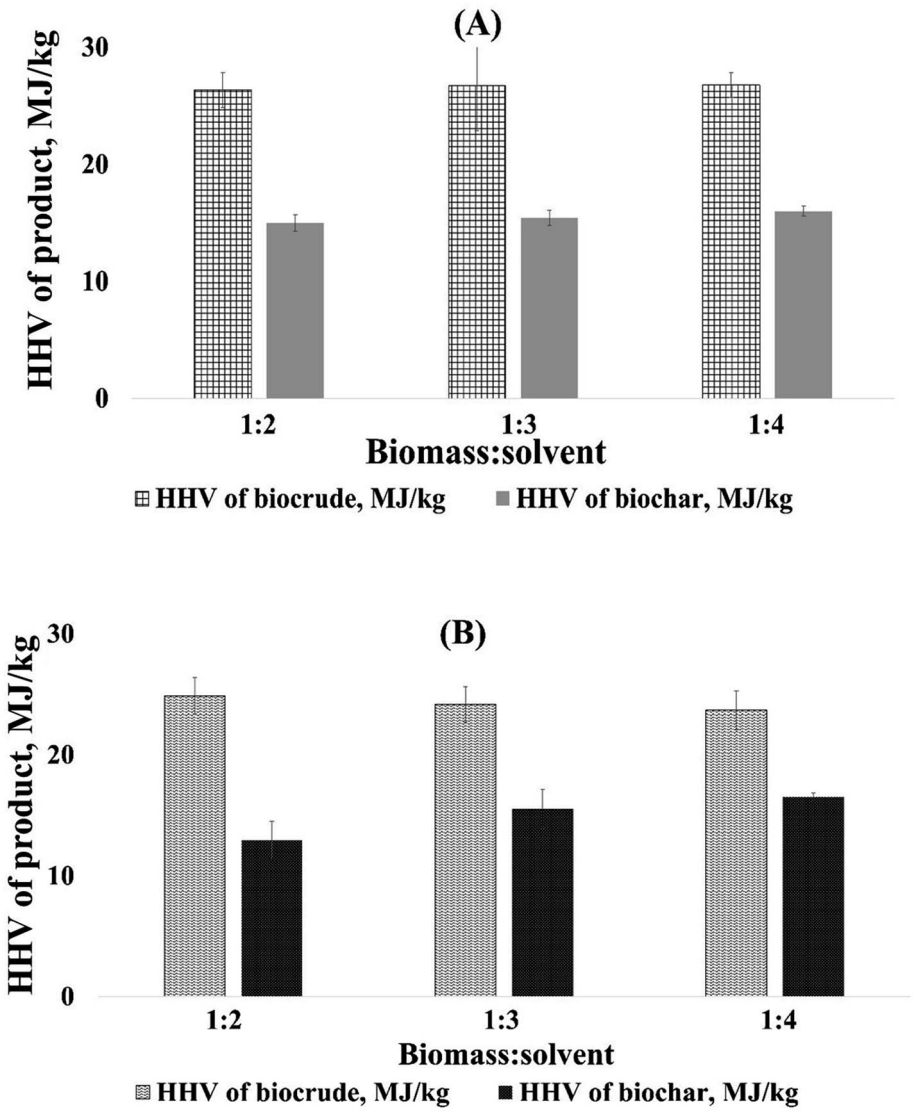

Fig. 4 HHV of (A) CLPU and (B) CLPE biocrude and biochar at 260 °C and different biomass-to-solvent ratios.

value.[15,43] The HHV of biocrude from the CLPE biomass was slightly lower than that from CLPU biomass, as per the findings of the authors. This might be owing to the occurrence of a higher content of oxygen in this biocrude.[54] But it is worth noting that these HHV values were still higher than the corresponding raw biomasses.

3.3.2 Chemical analysis. Hereafter, the biocrude obtained from the liquefaction of CLPU at 1 : 2, 1 : 3, and 1 : 4 biomass-to-solvent ratios have been denoted as BPU 2, BPU 3, and BPU 4, respectively. Similarly, the biocrude from CLPE at similar biomass-to-solvent ratios have been denoted as BPE 2, BPE 3, and BPE 4, respectively. The FTIR spectra of the biocrude has been depicted in Fig. 5 and gave an account of the functional groups present in them. The broad peaks in the spectra in the range of 3200–3400 cm^{-1} corresponded to phenolic compounds owing to the presence of the O–H stretching vibration of hydroxyl groups.[5] The absorption peaks in the 3000–2800 cm^{-1} and 1460–1350 cm^{-1} range, corresponding to C–H stretching vibration, might have occurred due to methyl and methylene groups, and indicated the possibility of the presence of long chain alkanes.[56,57] The absorption peaks in between 1800–1586 cm^{-1} indicated C=O stretching vibration in carboxylic acids, esters, ketones, and aldehydes group.[58] C–O stretching and O–H bending of primary, secondary, tertiary alcohols, ester, phenol, and ether were evident from the peak at about 1020 cm^{-1}.[59] In addition to these, the peaks in the 800–740 cm^{-1} range specified the presence of single, polycyclic, and substituted aromatic groups.[60] Although the functional groups were almost similar in the FTIR spectra of both biomasses, the slight increase in the intensity of peaks owing to C–H stretching while decrease in the intensities of O–H, C–O, and C=O peaks in the biocrude of CLPU put forward the decline in the oxygen groups. This was evident from the higher HHV of the biocrude obtained from CLPU in comparison to CLPE.

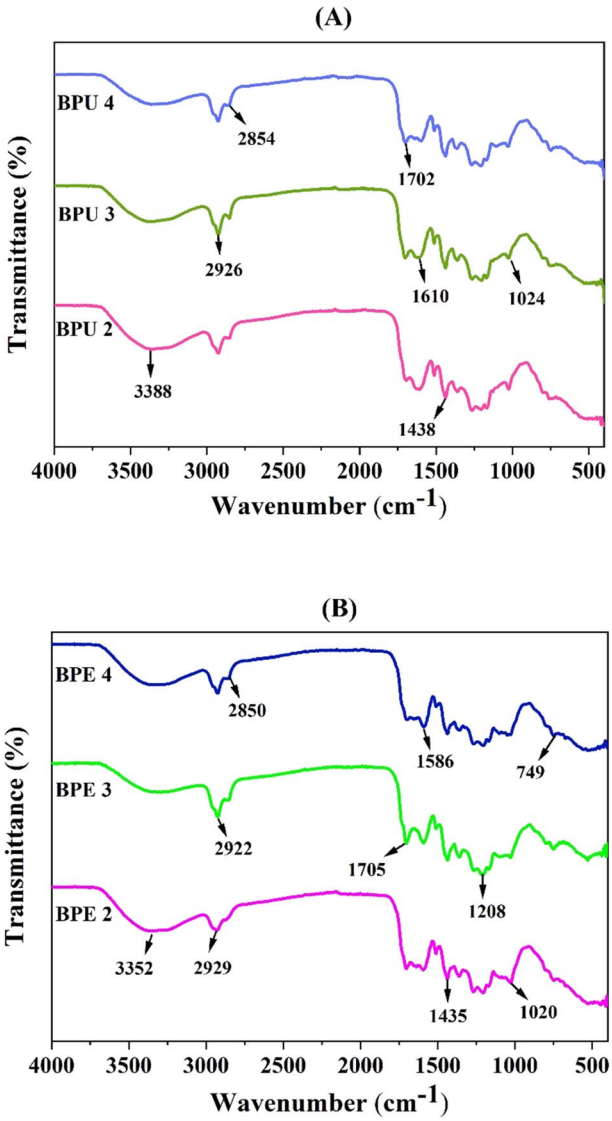

Fig. 5 FTIR spectra of (A) CLPU and (B) CLPE biocrude at different biomass-to-solvent ratios.

The molecular composition of the biocrude from the liquefaction of CLPU and CLPE were examined by GC-MS analysis. The compounds corresponding to the major peaks were identified from the NIST library, as shown in Table 4. Major compounds were seen to be lying within the range of C_2 to C_{38} groups. The biocrude mainly consisted of esters, fatty acids, phenols, alcohols, ketones, hydrocarbons, and N-containing compounds, as already evident from their FTIR (Fig. 5) and NMR studies. The presence of esters could be credited to the breakdown of hemicellulose and cellulose.[61] The methylated esters designated the contribution of hydrogen-donor methanol in liquefaction by esterification/methanolysis.[62] However, the biocrude composition was also highly dependent on the operation conditions and type of feedstock being used.[63] Biocrude obtained from the liquefaction of microalgae was generally high in N & O containing compounds along with fatty acids, which was contrary to low N-containing compounds in this case. The same has been found and reported in liquefaction studies with other citrus fruit wastes and rendered this biocrude as fruitful for further upgradation as well as downstream applications.[35] The breakage of benzoylether and β-aryl bonds in lignin led to its decomposition and formation of phenolic compounds in biocrude.[64] The low content of phenols indicated the less harmful and noxious nature of the biocrude. The hydrolysis of lipids in the feedstock promoted by the *in situ* hydrogen donation by methanol[22] led to the formation of long chain hydrocarbons in them.[35] The high temperature solvent environment led to the dehydration of hemicellulose and aided the formation of ketones as seen in the GC-MS. Meanwhile, compounds with higher aromatic content were formed from the dehydration and aromatization of cellulose and hemicellulose structural units.[65] These results were comparable to the literature that signified a high share of hydrocarbons and esters with low N-containing compounds and phenols in the liquefaction biocrude.[66,67] However, due to instrumental limitations, GC-MS was able to give only partial information about the probable chemical compounds in the biocrude,

Table 4 Major compounds identified through GC-MS analysis of biocrude obtained from the liquefaction of CLPU and CLPE at different biomass-to-solvent ratios

Compounds	Molecular formula	Chemical class	BPU 2		BPU 3		BPU 4		BPE 2		BPE 3		BPE 4	
			RT (min)	Area (%)	RT (min)	Area (%)	RT (min)	Area (%)	RT (min)	Area (%)	RT (min)	Area (%)	RT (min)	Area (%)
Ethanamine	C_2H_7N	Amines, aliphatic	8.133	4.332	—	—	—	—	—	—	—	—	—	—
Furan, 2-methoxy-	$C_5H_6O_2$	Alkyl aryl ethers	8.629	23.989	—	—	6.909	8.073	—	—	6.914	8.778	6.909	10.356
Cyclobutanecarboxylic acid	$C_5H_8O_2$	Organic acid	—	—	—	—	—	—	—	—	—	—	—	—
Cyclopentane-1,2-diol	$C_5H_{10}O_2$	Cyclopentanols	—	—	—	—	—	—	—	—	5.279	8.021	—	—
Ethanol, pentamethyl-	$C_7H_{16}O$	Alcohol	9.469	12.891	7.664	9.320	7.669	5.163	—	—	7.669	5.814	—	—
2-Azetidinone, 3,3,4,4-tetramethyl-	$C_7H_{13}NO$	Ketone	—	—	—	—	5.289	11.319	—	—	—	—	—	—
Azetidine, 2,2,3,3-tetramethyl-	$C_7H_{15}N$	Amine	—	—	—	—	—	—	—	—	—	—	5.279	8.903
3-Methyl-2-(2-oxopropyl)furan	$C_8H_{10}O_2$	Heteroatomic compounds	—	—	5.013	4.232	—	—	15.122	4.282	—	—	—	—
5-Hepten-2-amine, *N*,6-dimethyl-	$C_9H_{19}N$	Amine	—	—	—	—	5.013	7.379	—	—	—	—	—	—
2-Octanol, 2,6-dimethyl-	$C_{10}H_{22}O$	Fatty alcohols	—	—	—	—	—	—	—	—	—	—	7.674	7.021
2-Octene, 4-ethyl-	$C_{10}H_{20}$	Unsaturated aliphatic hydrocarbons	10.574	0.293	—	—	—	—	—	—	—	—	—	—
Benzaldehyde, 4-(1-methylethyl)-	$C_{10}H_{12}O$	Aromatic monoterpenoids	—	—	—	—	—	—	—	—	32.401	1.374	—	—
2-Ethylmethcathinone	$C_{12}H_{17}NO$	Alkyl-phenylketones	8.023	2.047	—	—	—	—	—	—	—	—	—	—
Bicyclo[4.1.0]heptane, 7-pentyl-	$C_{12}H_{22}$	Polycyclic hydrocarbons	31.813	0.363	—	—	—	—	—	—	—	—	—	—
4-Hydroxyphenyl-4-methyl-2-pentanone	$C_{12}H_{16}O_2$	Ketone	41.417	0.393	—	—	—	—	—	—	—	—	—	—
Undecanoic acid, 10-methyl-, methyl ester	$C_{13}H_{26}O_2$	Fatty acid methyl esters	—	—	—	—	28.898	2.189	—	—	—	—	—	—
Methyl 11-methyl-dodecanoate	$C_{14}H_{28}O_2$	Fatty acid methyl esters	—	—	—	—	—	—	—	—	—	—	28.898	1.892
4-*tert*-Octylphenol	$C_{14}H_{22}O$	Phenol	38.511	0.349	—	—	—	—	—	—	—	—	—	—
7,11-Hexadecadienal	$C_{16}H_{28}O$	Fatty aldehydes	—	—	—	—	—	—	—	—	31.315	1.752	—	—
1-Pentadecene, 2-methyl-	$C_{16}H_{32}$	Branched unsaturated hydrocarbons	—	—	—	—	—	—	—	—	—	—	5.013	7.326
1-Nonylcycloheptane	$C_{16}H_{32}$	Polycyclic hydrocarbons	31.733	0.601	—	—	—	—	—	—	—	—	—	—
(1*S*,15*S*)-Bicyclo[13.1.0]hexadecan-2-one	$C_{16}H_{28}O$	Ketones	—	—	31.289	1.123	—	—	—	—	—	—	—	—
Orcinyl di-angelate	$C_{17}H_{20}O_4$	Ester	—	—	6.904	13.229	—	—	—	—	—	—	—	—
9,12-Hexadecadienoic acid, methyl ester	$C_{17}H_{30}O_2$	Fatty acid methyl esters	—	—	—	—	—	—	—	—	—	—	31.289	1.706
6-Octadecenoic acid	$C_{18}H_{34}O_2$	Fatty acid (petroselinic)	—	—	—	—	—	—	12.496	2.631	—	—	—	—
Hexestrol TMS derivative	$C_{18}H_{22}O_2$	Phenol	41.627	0.401	—	—	—	—	—	—	—	—	—	—
Methyl 9,10-octadecadienoate	$C_{19}H_{34}O_2$	Fatty acid ester	—	—	—	—	31.219	1.670	—	—	—	—	—	—
11,14-Octadecadienoic acid, methyl ester	$C_{19}H_{34}O_2$	Fatty acid methyl esters (FAME)	31.658	0.5	—	—	—	—	—	—	—	—	—	—
11,14-Octadecadienoic acid, methyl ester	$C_{19}H_{34}O_2$	Fatty acid methyl esters	—	—	—	—	—	—	—	—	31.245	1.254	31.224	1.671
Butyl 9-hexadecenoate	$C_{20}H_{38}O_2$	Fatty acid esters	—	—	—	—	—	—	—	—	5.013	6.108	—	—
Methyl 9-eicosenoate	$C_{21}H_{40}O_2$	Fatty acid methyl esters	—	—	—	—	31.294	2.107	—	—	—	—	31.349	1.326
I-Propyl 11,12-methylene-octadecanoate	$C_{22}H_{42}O_2$	Lipid derivative	—	—	—	—	—	—	13.532	3.803	—	—	—	—
Methyl 11-docosenoate	$C_{23}H_{44}O_2$	Fatty acid ester	—	—	—	—	31.354	1.743	—	—	—	—	—	—
2,6,10,14-Tetramethyl-7-(3-methylpent-4-enylidene) pentadecane	$C_{25}H_{48}$	Alkyne	—	—	—	—	—	—	10.866	3.935	—	—	—	—
Hexacosyl acetate	$C_{28}H_{56}O_2$	Long chain fatty acid	—	—	—	—	—	—	20.380	3.303	—	—	—	—

Table 4 (*Contd.*)

Compounds	Molecular formula	Chemical class	BPU 2		BPU 3		BPU 4		BPE 2		BPE 3		BPE 4	
			RT (min)	Area (%)	RT (min)	Area (%)	RT (min)	Area (%)	RT (min)	Area (%)	RT (min)	Area (%)	RT (min)	Area (%)
Heptacosanoic acid, 25-methyl-, methyl ester	$C_{29}H_{58}O_2$	Fatty acid methyl esters (FAME)	29.267	0.637	28.893	1.005	—	—	—	—	—	—	—	—
(*Z*)-Decyl icos-9-enoate	$C_{30}H_{58}O_2$	Wax monoesters	—	—	—	—	—	—	16.978	3.297	—	—	—	—
9-Octadecenoic acid (*Z*)-, octadecyl ester	$C_{36}H_{70}O_2$	Fatty acid methyl esters (FAME)	—	—	—	—	—	—	16.798	5.192	—	—	—	—
Z,*Z*-6,28-Heptatriactontadien-2-one	$C_{37}H_{70}O$	Long chain ketone	—	—	31.219	1.117	—	—	14.237	4.667	—	—	—	—
Oleic acid, eicosyl ester	$C_{38}H_{74}O_2$	Wax monoesters	—	—	—	—	—	—	15.358	6.640	—	—	—	—

such as the identification of some high boiling point compounds, remained absent because of the temperature limit of the GC-MS. Similarly, compounds with low boiling point also remained unaccounted for due to their losses during biocrude separation. The confirmation of the functional groups and assignments by means of chemical shift in ppm was obtained by proton NMR technique.[68] The ^{1}H NMR of the biocrude from the liquefaction of CLPU and CLPE presented peaks at a chemical shift of 7.26 ppm, which corresponded to chloroform-D solvent used in the analysis. However, the peak at 0 ppm could be considered as a standard for tetramethylsilane (TMS), which is the default in NMR systems.[6] Aliphatic protons attached to carbon atoms (alkanes) were evident in peaks in the range of 0–1.5 ppm.[69] This indicated the fatty acids and hydrocarbons in the biocrude and were seen to have consistency with the GC-MS results discussed above. The peaks in the range of 1.5–3 ppm indicated the presence of aliphatic protons attached to unsaturated heteroatom or carbon.[70] On the other hand, the

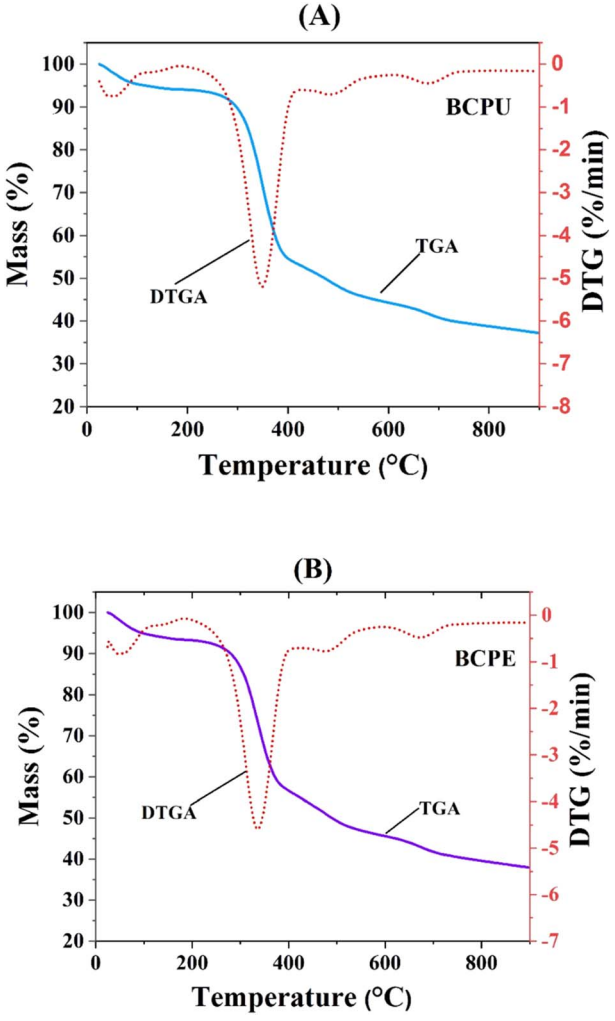

Fig. 6 Thermogravimetric analysis (TGA) and differential thermogravimetry (DTG) plot of (A) CLPU and (B) CLPE biochar.

peaks at 3–4.5 ppm corresponded to protons bound to carbon of ethers, alcohols, and esters.[54] The consumption of methanol in the liquefaction reaction boosted the formation of alcoholic and esters compounds, which was verified from the FTIR spectra of the biocrude from both biomasses. A low proton distribution in the range of 4.5–6 ppm was an indication of weak carbohydrate and methoxy functionalities.[15]

3.4 Analysis of biochar

Fig. 6 showed the TGA and DTG plots of biochar from the liquefaction of CLPU and CLPE at all three biomass-to-solvent ratios mixed together, which were denoted as BCPU and BCPE, respectively. The moisture loss from biomolecules and changes in the lipid structure were indicated by the mass loss in the temperature range of 40–200 °C. The decomposition of carbohydrates was evident in the range of 200–400 °C. However, above 400 °C, the mass loss pointed toward the complete decomposition and oxidation of organic matter.[71] The highest weight loss rate of biochar obtained from liquefaction in methanol was observed at 350–357 °C, suggesting that the complete degradation of cellulose and hemicellulose in CLPU and CLPE had not occurred. The TGA curves of the biochar indicated their high thermal stability.[72] The HHV of the biochar, as shown in Table 3, indicated a maximum at 16.98 MJ kg^{-1} for biochar from CLPU, while it was in the range of 14.94–16.5 MJ kg^{-1} for CLPE biochar. Specifically, the HHV of CLPU biochar marginally decreased with increasing biomass-to-solvent ratio, and the opposite was true for the case of CLPE biochar. Nevertheless, the HHV of CLPU biochar was higher than that of CLPE biochar for any fixed biomass-to-solvent ratio. These values signified their ability to be used as a potential feedstock in biorefineries.[54] Their porous structure verified their applications in wastewater bioremediation, soil treatment, and as a catalyst for biomass conversion.[73–75] The powder X-ray diffraction (XRD) technique was utilized to determine the crystallinity of the biomass and dry biochar samples by taking into account the changes in the crystalline structure of cellulose by the interruption of the hydrogen bonding of cellulose chains occurring due to liquefaction.[76] Fig. 7 illustrated the XRD pattern for the CLPU and CLPE biomasses along with their corresponding liquefaction biochar obtained at 1 : 2, 1 : 3, and 1 : 4 biomass-to-solvent ratios, which were termed as BCPU 2, BCPU 3, and BCPU 4 (for CLPU biomass), while they were named as BCPE 2, BCPE 3, and BCPE 4 (for CLPE biomass) respectively. The XRD pattern of both CLPU and CLPE biomass showed two discrete peaks for cellulose at $2\theta = 15°$ and 22°.[77,78] The presence of peaks at $2\theta =$ 24° and 26° showed cellulose and lignin breakdown in the process and implied turbostratic and amorphous carbon.[79] These carbon peaks signified biochar formation by cellulose and lignin decomposition during liquefaction.[80] The biomass structure was composed of multifaceted compounds; however, despite their breakdown due to thermochemical conversion processes to produce biochar, the biochar samples retained their crystalline nature partially, which was visible from their XRD plots.[54,81]

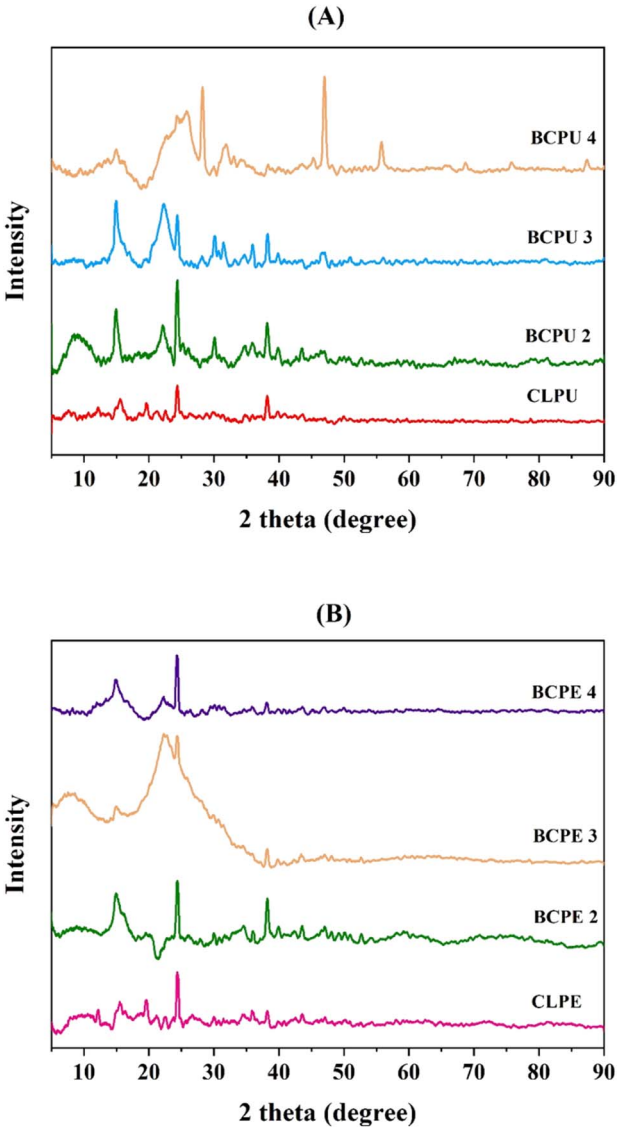

Fig. 7 X-ray diffractrogram of (A) CLPU and (B) CLPE biomass and biochar obtained by liquefaction at different biomass-to-solvent ratios.

The surface morphology of the CLPU and CLPE biomasses along with their corresponding mixed biochar obtained at all three biomass-to-solvent ratios have been studied by FESEM (at (i) 2k×, (ii) 5k×, and (iii) 10k× resolutions), as depicted in Fig. 8. It was evident from the images that the biomass was a lumpy, dense solid matrix, having a fibrous structure.[5] However, after liquefaction, the changes in the surface were visible from the images of the biochar. Due to cellulose and hemicellulose decomposition, the structure of the cell was broken, leading to the development of cracks on the surface with certain pores over them.[82] Certain agglomerations were observed on the biochar surface owing to crosslinking induced by dehydration between the hemicellulose and cellulose molecules. The mineral residues from biomass liquefaction were apparent from the magnified FESEM images, showing small particle deposits on the biochar surface.[83]

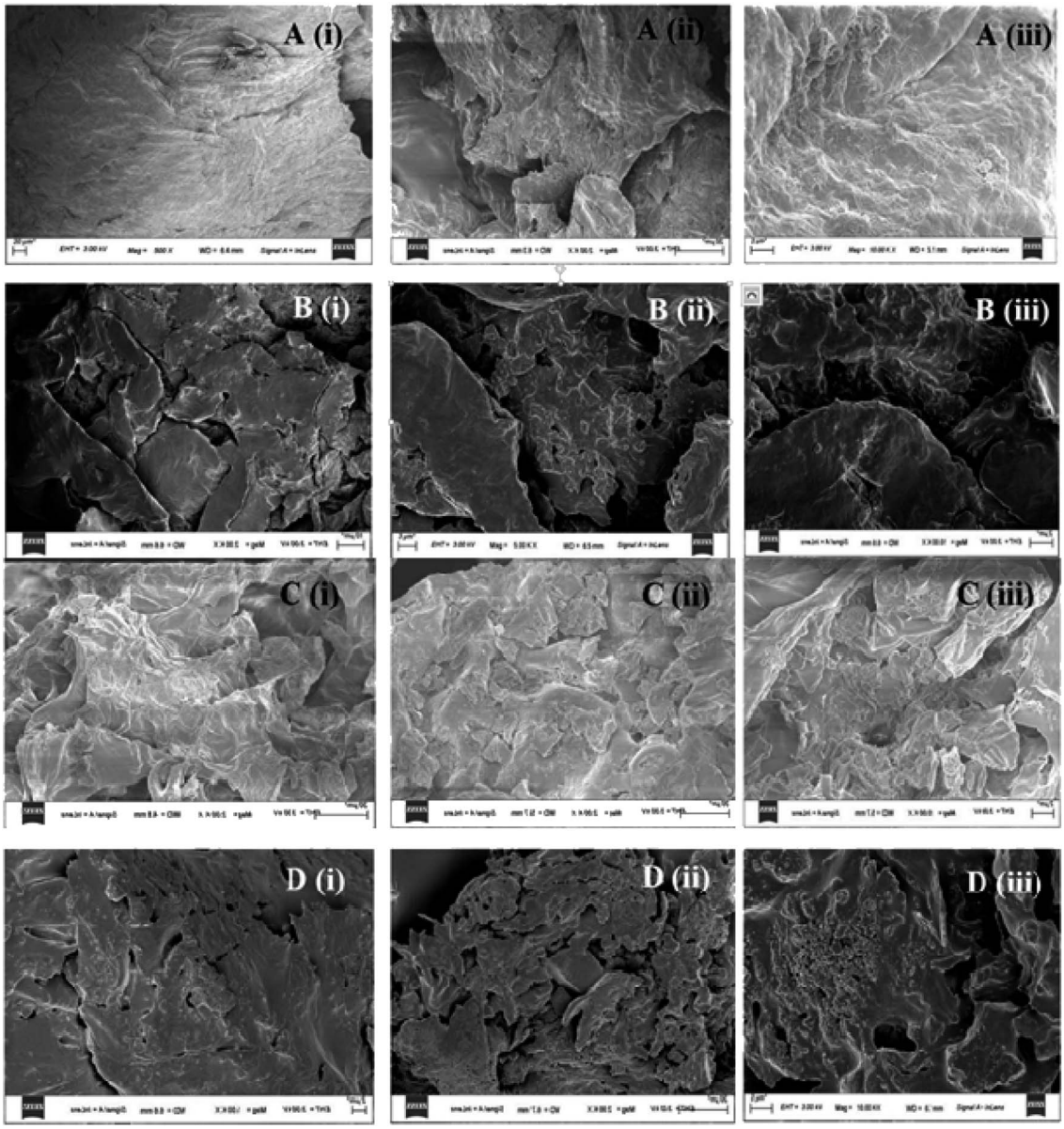

Fig. 8 (A(i–iii)) FESEM images of CLPU biomass; (B(i–iii)) FESEM images of biochar obtained by the liquefaction of CLPU biomass; (C(i–iii)) FESEM images of CLPE biomass; and (D(i–iii)): FESEM images of biochar obtained by the liquefaction of CLPE biomass (at (i) 2k×, (ii) 5k×, and (iii) 10k× resolutions each).

4. Conclusion

The authors were able to achieve need of the hour waste management by the liquefaction of fruit wastes (both pulp and peel) of *Citrus limetta* in hydrogen-donor methanol solvent. This highly volatile biomass was responsible for high biocrude yield, with a maximum of 12.5 wt% from *Citrus limetta* peel, which was higher than the thermochemical conversion of other citrus fruit waste biomasses reported in the literature. This yield was also aided by the high pressure of the reaction to achieve better decomposition of the biomass by effective solvent penetration. The density of *Citrus limetta* pulp filtrates and remaining methanol solvent (MSR) were higher than that of *Citrus limetta* peel, irrespective of the biomass-to-solvent ratios. On the other hand, both their viscosities were found to decrease with increasing biomass-to-solvent ratios. The viscosities of the remaining methanol solvent (MSR) for both these cases were, however, much higher than pure methanol solvent, indicating the presence of some lighter fuel fractions and/or methanol soluble components of the filtrate in them. From the fuel potential point of view, almost a neutral pH of 6.2 to 7.2 of the *Citrus limetta* pulp and *Citrus limetta* peel filtrates was a positive outcome. It was found that apart from the biomass-to-solvent ratio, several other factors contributed in obtaining an optimized quantity and quality of the products. The decrease in C–O, O–H, and C=O peaks in the FTIR of *Citrus limetta* pulp biocrude justified its maximum HHV of 26.76 MJ kg^{-1} in

comparison to *Citrus limetta* peel biocrude. GC-MS analysis showed the existence of esters in the biocrude that were a consequence of the esterification of the hydrogen-donor methanol solvent. Moreover, low N-containing compounds in the biocrude, as found from GC-MS, depicted its possibility to be fruitful in further upgradation and downstream applications. The biocrude also consisted of compounds of higher aromatic content due to the dehydration and aromatization of cellulose and hemicellulose. The NMR peaks at chemical shift of 0–1.5 ppm indicated the presence of fatty acids and hydrocarbons, which was in accordance with the GC-MS results. Biochar of high thermal stability with maximum HHV of 16.98 MJ kg^{-1} was found from *Citrus limetta* pulp biomass and signified their potential to be used in bio-refineries. The carbon peaks in the XRD of biochar as well as their FESEM images were responsible for establishing the occurrence of decomposition of hemicellulose, cellulose, and lignin in the liquefaction process. Finally, based on the properties of the products, it can be said that the present biocrude and biochar obtained at 260 °C from fruit wastes were superior in comparison to similar works with other citrus fruit waste biomasses reported in the literature. The authors intend to explore the qualitative improvement of the biocrude by the diversification of the reaction parameters as well as catalytic upgrading of the products. The biochar could also be further processed for utilization as low-cost adsorbents in soil remediation as well as catalysts for thermochemical conversion technologies.

Author contributions

Sneha Acharya: investigation, methodology, writing – original draft. Nanda Kishore: conceptualization, methodology, supervision, writing – reviewing and editing, resources, project administration, funding acquisition.

Conflicts of interest

The authors hereby declare that they have no known competing financial interests or personal relationships that could have appeared to influence the work reported in this paper.

Acknowledgements

Authors convey their gratitude towards the Analytical Lab, Department of Chemical Engineering, IIT Guwahati for granting the permission for usage of the required analytical instruments for this study. Authors acknowledge the XRD and FESEM (Gemini) facilities availed from Central Instruments Facility, IIT Guwahati. They are also grateful to Biotech Park, Guwahati for study of the biomass sample by CHNS elemental analyzer and biocrude by Gas Chromatography Mass Spectrometry (GC-MS).

References

1 I. U. Khan, A. Haleem and A. U. Khan, *RSC Adv.*, 2022, **12**, 21223–21234.
2 S. Anouti, G. Haarlemmer, M. Déniel and A. Roubaud, *Energy Fuels*, 2016, **30**, 398–406.
3 Y. Wang, X. Gu, Y. Huang, Z. Ding, Y. Chen and X. Hu, *RSC Adv.*, 2022, **12**, 19318–19326.
4 K. Alper, K. Tekin, S. Karagöz and A. J. Ragauskas, *Sustainable Energy Fuels*, 2020, **4**, 4390–4414.
5 G. Ahmed, S. Acharya, H. Kawale, A. Singh, N. Kishore and S. Pal, *Fuel*, 2020, **280**, 118574.
6 S. Gupta, H. D. Kawale, G. Ahmed, S. Acharya and N. Kishore, *Curr. Res. Green Sustainable Chem.*, 2021, **4**, 100062.
7 A. R. K. Gollakota, H. D. Kawale, N. Kishore and S. Gu, *Renewable Sustainable Energy Rev.*, 2018, **98**, 515–517.
8 D. Castello and T. H. Pedersen, *Energies*, 2018, **11**, 3165.
9 A. R. K. Gollakota, N. Kishore and S. Gu, *Renewable Sustainable Energy Rev.*, 2018, **81**, 1378–1392.
10 H. Sudibyo, M. Pecchi and J. W. Tester, *Sustainable Energy Fuels*, 2022, **6**, 2314–2329.
11 A. Yerrayya, A. K. Shree Vishnu, S. Shreyas, S. R. Chakravarthy and R. Vinu, *Energies*, 2020, **13**, 1–19.
12 W. Prins, F. Ronsse, W. Brilman and D. Lo, *Biomass Bioenergy*, 2013, **53**, 113–127.
13 B. Biswas, A. Arun Kumar, Y. Bisht, B. B. Krishna, J. Kumar and T. Bhaskar, *Energy*, 2021, **217**, 119330.
14 J. Zhang and Y. Zhang, *Energy Fuels*, 2014, **28**, 5178–5183.
15 Q. Li, D. Liu, L. Song, P. Wu, Z. Yan and M. Li, *Fuel*, 2016, **164**, 94–98.
16 D. Mahesh, S. Ahmad, R. Kumar, S. R. Chakravarthy and R. Vinu, *Bioresour. Technol.*, 2021, **339**, 125537.
17 H. Feng, B. Zhang, Z. He, S. Wang, O. Salih and Q. Wang, *Energy*, 2018, **155**, 1093–1101.
18 B. Zhao, H. Wang, S. Xu, L. Qian, H. Li, J. Gao, G. Zhao, M. B. Ray and C. C. Xu, *Fuel*, 2022, **307**, 121930.
19 R. Singh, T. Bhaskar and B. Balagurumurthy, *Process Saf. Environ. Prot.*, 2015, **93**, 154–160.
20 B. de Caprariis, P. De Filippis, A. Petrullo and M. Scarsella, *Fuel*, 2017, **208**, 618–625.
21 J. Wang, G. Zeng, H. Huang, X. Pei, H. Li, Z. Liu and M. Cong, *Energy*, 2011, **36**, 6406–6412.
22 B. Zhao, H. Wang, S. Xu, L. Qian, H. Li, J. Gao, G. Zhao, M. B. Ray and C. C. Xu, *Fuel*, 2022, **307**, 121930.
23 K. Alper, Y. Y. Wang, X. Meng, K. Tekin, S. Karagoz and A. J. Ragauskas, *Sustainable Energy Fuels*, 2021, **5**, 5445–5453.
24 D. Zhou, S. Zhang, H. Fu and J. Chen, *Energy Fuels*, 2012, **26**, 2342–2351.
25 Q. Li, D. Liu, X. Hou, P. Wu, L. Song and Z. Yan, *Bioresour. Technol.*, 2016, **219**, 281–288.
26 Z. Zhang, I. M. O'Hara, S. Mundree, B. Gao, A. S. Ball, N. Zhu, Z. Bai and B. Jin, *Curr. Opin. Biotechnol.*, 2016, **38**, 97–105.
27 K. Jõgi and R. Bhat, *Sustainable Chem. Pharm.*, 2020, **18**, 100326.
28 *International Plant Names Index*, **https://www.ipni.org/n/771956-1**, accessed October, 2022.
29 D. Rivera, A. Bermúdez, C. Obón, F. Alcaraz, S. Ríos, J. Sánchez-Balibrea, P. Pablo Ferrer-Gallego and R. Krueger, *Sci. Hortic.*, 2022, **293**, 110688.
30 W. H. Chen, Y. Y. Lin, H. C. Liu and S. Baroutian, *Energy*, 2020, **199**, 117438.

31 M. J. Stablein, A. Aierzhati, J. Watson, B. Si and Y. Zhang, *Bioresour. Technol. Rep.*, 2020, **12**, 100555.
32 B. Zhang, J. Chen, S. Kandasamy and Z. He, *Energy*, 2020, **193**, 116645.
33 S. O. Dahunsi, *Energy*, 2019, **185**, 1017–1031.
34 Y. H. Chan, A. T. Quitain, S. Yusup, Y. Uemura, M. Sasaki and T. Kida, *J. Energy Inst.*, 2019, **92**, 535–541.
35 B. Zhang, J. Chen, H. Chen and S. Kandasamy, *Renewable Energy*, 2019, **143**, 512–519.
36 S. Hongthong, S. Raikova, H. S. Leese and C. J. Chuck, *Waste Manage.*, 2020, **102**, 351–361.
37 R. Saha, K. Mukherjee, I. Saha, A. Ghosh, S. K. Ghosh and B. Saha, *Res. Chem. Intermed.*, 2013, **39**, 2245–2257.
38 S. Shakoor and A. Nasar, *J. Taiwan Inst. Chem. Eng.*, 2016, **66**, 154–163.
39 Poonam and N. Kumar, *Environ. Dev. Sustain.*, 2020, **22**, 4379–4406.
40 M. M. Musthafa, *Energy Sources, Part A*, 2016, **38**, 2994–3000.
41 V. Sukumar, V. Manieniyan, R. Senthilkumar and S. Sivaprakasam, *Renewable Energy*, 2020, **146**, 309–315.
42 S. Abidi, A. Trabelsi and N. Boudhrioua, *J. Mater. Cycles Waste Manage.*, 2022, in press, DOI: **10.1007/s10163-022-01527-1**.
43 H. Zeb, A. Riaz and J. Kim, *J. Supercrit. Fluids*, 2017, **120**, 65–74.
44 M. K. Jindal and M. K. Jha, *RSC Adv.*, 2016, **6**, 41772–41780.
45 R. Li, B. Li, T. Yang, X. Kai, W. Wang, Y. Jie, Y. Zhang and G. Chen, *Bioresour. Technol.*, 2015, **198**, 94–100.
46 S. Brand, R. F. Susanti, S. K. Kim, H.-s. Lee, J. Kim and B. I. Sang, *Energy*, 2013, **59**, 173–182.
47 J. Zhang, W. T. Chen, P. Zhang, Z. Luo and Y. Zhang, *Bioresour. Technol.*, 2013, **133**, 389–397.
48 G. Yu, Y. Zhang, L. Schideman, T. Funk and Z. Wang, *Energy Environ. Sci.*, 2011, **4**, 4587–4595.
49 A. Mehrabadi, R. Craggs and M. M. Farid, *Bioresour. Technol.*, 2017, **224**, 255–264.
50 L. C. Cardenas Velandia, A. E. Fontaine, D. Loquet, R. Checa, C. Lorentz, B. Bujoli, N. Guilhaume, C. Geantet, E. Chailleux, C. Queffélec and D. Laurenti, *J. Cleaner Prod.*, 2021, **322**, 129024.
51 P. D. Pathak, S. A. Mandavgane and B. D. Kulkarni, *Curr. Sci.*, 2017, **113**, 444–454.
52 A. C. Gowman, M. C. Picard, A. Rodriguez-Uribe, M. Misra, H. Khalil, M. Thimmanagari and A. K. Mohanty, *BioResources*, 2019, **14**, 3210–3230.
53 H. D. Kawale and N. Kishore, *J. Energy Resour. Technol.*, 2020, **142**(8), 082306.
54 S. Acharya and N. Kishore, *Int. J. Sustainable Energy*, 2022, in press, DOI: **10.1080/14786451.2022.2140157**.
55 J. A. Ramirez, R. J. Brown and T. J. Rainey, *Energies*, 2015, **8**, 6765–6794.
56 R. Li, Z. Ma, T. Yang, B. Li, L. Wei and Y. Sun, *J. Supercrit. Fluids*, 2018, **138**, 115–123.
57 C. Xu and T. Etcheverry, *Fuel*, 2008, **87**, 335–345.
58 H. D. Kawale and N. Kishore, *Renewable Energy*, 2021, **173**, 223–236.
59 B. Zhang, H. Feng, Z. He, S. Wang and H. Chen, *Energy Convers. Manage.*, 2018, **159**, 204–212.
60 Y. Chen, Y. Wu, P. Zhang, D. Hua, M. Yang, C. Li, Z. Chen and J. Liu, *Bioresour. Technol.*, 2012, **124**, 190–198.
61 R. Li, B. Li, X. Kai and T. Yang, *Fuel Process. Technol.*, 2017, **167**, 363–370.
62 Z. Bi, J. Zhang, E. Peterson, Z. Zhu, C. Xia, Y. Liang and T. Wiltowski, *Fuel*, 2017, **188**, 112–120.
63 A. Gollakota and P. E. Savage, *ACS Sustainable Chem. Eng.*, 2018, **6**, 9018–9027.
64 S. Karagöz, T. Bhaskar, A. Muto, Y. Sakata, T. Oshiki and T. Kishimoto, *Chem. Eng. J.*, 2005, **108**, 127–137.
65 D. Liu, Q. Li, A. Zhao, L. Song, P. Wu and Z. Yan, *Chem. Eng. J.*, 2015, **279**, 921–928.
66 S. Koley, M. S. Khadase, T. Mathimani, H. Raheman and N. Mallick, *Energy Convers. Manage.*, 2018, **163**, 111–121.
67 W. H. Chen, Y. Y. Lin, H. C. Liu, T. C. Chen, C. H. Hung, C. H. Chen and H. C. Ong, *Appl. Energy*, 2019, **237**, 283–291.
68 H. D. Kawale and N. Kishore, *Energy*, 2020, **203**, 117921.
69 C. A. Mullen, G. D. Strahan and A. A. Boateng, *Energy Fuels*, 2009, **23**, 2707–2718.
70 H. D. Kawale and N. Kishore, *J. Therm. Anal. Calorim.*, 2022, **147**, 2969–2983.
71 S. Masoumi, P. E. Boahene and A. K. Dalai, *Energy*, 2021, **217**, 119344.
72 Z. qian Pan, H. jun Huang, C. fei Zhou, X. feng Xiao, X. wu He, F. ying Lai and J. bo Xiong, *J. Anal. Appl. Pyrolysis*, 2018, **136**, 186–198.
73 N. Hassan, R. Abdullah, T. Khadiran, P. Elham and P. Vejan, *Biomass Convers. Biorefin.*, 2021, in press, DOI: **10.1007/s13399-021-01797-z**.
74 X. Xiong, I. K. M. Yu, L. Cao, D. C. W. Tsang, S. Zhang and Y. S. Ok, *Bioresour. Technol.*, 2017, **246**, 254–270.
75 Y. Shen, J. L. Linville, M. Urgun-Demirtas, R. P. Schoene and S. W. Snyder, *Appl. Energy*, 2015, **158**, 300–309.
76 N. Mosier, C. Wyman, B. Dale, R. Elander, Y. Y. Lee, M. Holtzapple and M. Ladisch, *Bioresour. Technol.*, 2005, **96**, 673–686.
77 W. Wu, M. Yang, Q. Feng, K. McGrouther, H. Wang, H. Lu and Y. Chen, *Biomass Bioenergy*, 2012, **47**, 268–276.
78 M. Keiluweit, P. S. Nico, M. Johnson and M. Kleber, *Environ. Sci. Technol.*, 2010, **44**, 1247–1253.
79 R. Kaur, P. Gera, M. K. Jha and T. Bhaskar, *Renewable Energy*, 2019, **141**, 1026–1041.
80 A. Oya and S. Otani, *Carbon*, 1981, **19**, 391–400.
81 H. D. Kawale and N. Kishore, *Energy*, 2019, **178**, 344–355.
82 S. Nizamuddin, H. A. Baloch, N. M. Mubarak, S. Riaz, M. T. H. Siddiqui, P. Takkalkar, M. M. Tunio, S. Mazari and A. W. Bhutto, *Waste Biomass Valorization*, 2019, **10**, 1957–1968.
83 R. Kaur, P. Gera, M. K. Jha and T. Bhaskar, *Renewable Energy*, 2019, **141**, 1026–1041.